NANO LETTERS

Letter

pubs.acs.org/NanoLett

Hot Electrons Do the Impossible: Plasmon-Induced Dissociation of H_2 on Au

Shaunak Mukherjee,[†,∥] Florian Libisch,[⊥] Nicolas Large,[‡,∥] Oara Neumann,[§,∥] Lisa V. Brown,[†,∥] Jin Cheng,[⊥] J. Britt Lassiter,[§,∥] Emily A. Carter,[⊥] Peter Nordlander,*[,‡,§,∥] and Naomi J. Halas*[,†,‡,§,∥]

[†]Department of Chemistry, [‡]Department of Electrical and Computer Engineering, [§]Department of Physics and Astronomy, and [∥]Laboratory for Nanophotonics, Rice University, 6100 Main Street, Houston, Texas 77005, United States

[⊥]Department of Mechanical and Aerospace Engineering, Program in Applied and Computational Mathematics, and the Andlinger Center for Energy and the Environment, Princeton University, Princeton, New Jersey 08544, United States

Supporting Information

ABSTRACT: Heterogeneous catalysis is of paramount importance in chemistry and energy applications. Catalysts that couple light energy into chemical reactions in a directed, orbital-specific manner would greatly reduce the energy input requirements of chemical transformations, revolutionizing catalysis-driven chemistry. Here we report the room temperature dissociation of H_2 on gold nanoparticles using visible light. Surface plasmons excited in the Au nanoparticle decay into hot electrons with energies between the vacuum level and the work function of the metal. In this transient state, hot electrons can transfer into a Feshbach resonance of an H_2 molecule adsorbed on the Au nanoparticle surface, triggering dissociation. We probe this process by detecting the formation of HD molecules from the dissociations of H_2 and D_2 and investigate the effect of Au nanoparticle size and wavelength of incident light on the rate of HD formation. This work opens a new pathway for controlling chemical reactions on metallic catalysts.

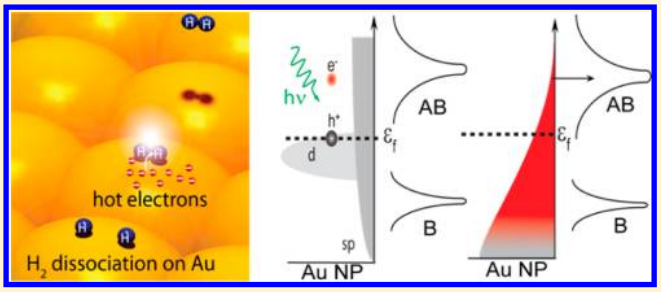

KEYWORDS: *Plasmon, hot electrons, photocatalysis, H_2 dissociation on Au surface, Au/TiO_2*

An important paradigm in the development of multifunctional materials for heterogeneous catalysis is enhanced reactivity and efficiency of catalysts for robust and prolonged use. Performing catalytic synthesis at low temperature and under ambient conditions ensures the longevity of active sites and reduces the possibility of high-temperature side reactions. In this context, noble metals have drawn significant attention due to their ability to couple light into chemical reactions. The strong coupling of metal nanoparticles with light at specific photon energies is due to the optical excitation of the collective electronic resonances of the metal, known as surface plasmons. The unique ability of noble metal nanoparticles to absorb and scatter light at specific wavelengths across a wide region of the electromagnetic spectrum, depending on the type of metal and nanoparticle geometry, makes them excellent candidate substrates for plasmon-enabled photochemistry.[1]

Plasmon-induced chemical processes have been gaining significantly increased attention due to their high throughput and low energy requirements. Examples of plasmon-induced reactions include liquid phase water splitting,[2−4] H_2 production from alcohol,[5,6] gas phase oxidation reactions,[7,8] and hydrocarbon conversion.[9] A limited set of heterogeneous gas phase experiments have been performed so far, emphasizing several different aspects of metal−adsorbate interactions that influence the rate of product formation. The adsorptive interaction and dissociation of H_2 on metal surfaces is one such reaction and is one of the most important reactions for heterogeneous catalysis. H_2 forms a strong nonpolarizable σ bond with a dissociation enthalpy of 436 kJ/mol (4.51 eV), an activation energy too large to surmount using a thermally induced process.

Recently it was demonstrated that plasmon-excited nanoparticles can be an efficient source of hot electrons (Figure 1a).[10−13] Following optical excitation, each plasmon quantum can decay either radiatively into a photon (scattering) or nonradiatively into an electron−hole pair (EHP). The branching ratio between these two channels depends on the size and radiance of the plasmon: for small nanoparticles or subradiant plasmon modes, the dominant decay channel is EHP formation. The most likely EHP formation occurs when the plasmon quantum excites an electron from the Fermi level to an occupied state below the vacuum level (Figure 1b). Because of their higher energy, hot electrons will extend further away from the nanoparticle than an equilibrium electron distribution (Figure 1c). If a nearby electron acceptor is present, hot electrons can transfer into its electronic states. This process can be quite efficient: hot electron transfer from a plasmonic nanostructure to a nearby graphene sheet was shown to have a quantum efficiency

Received: October 26, 2012
Revised: November 22, 2012
Published: November 29, 2012

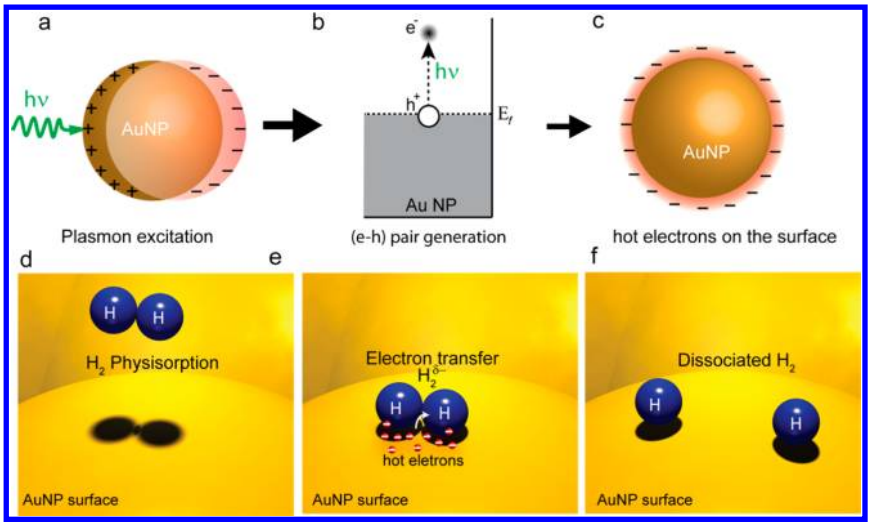

Figure 1. Schematics of plasmon-induced hot electron generation on AuNP and mechanistic representation of H_2 dissociation on the AuNP surface.

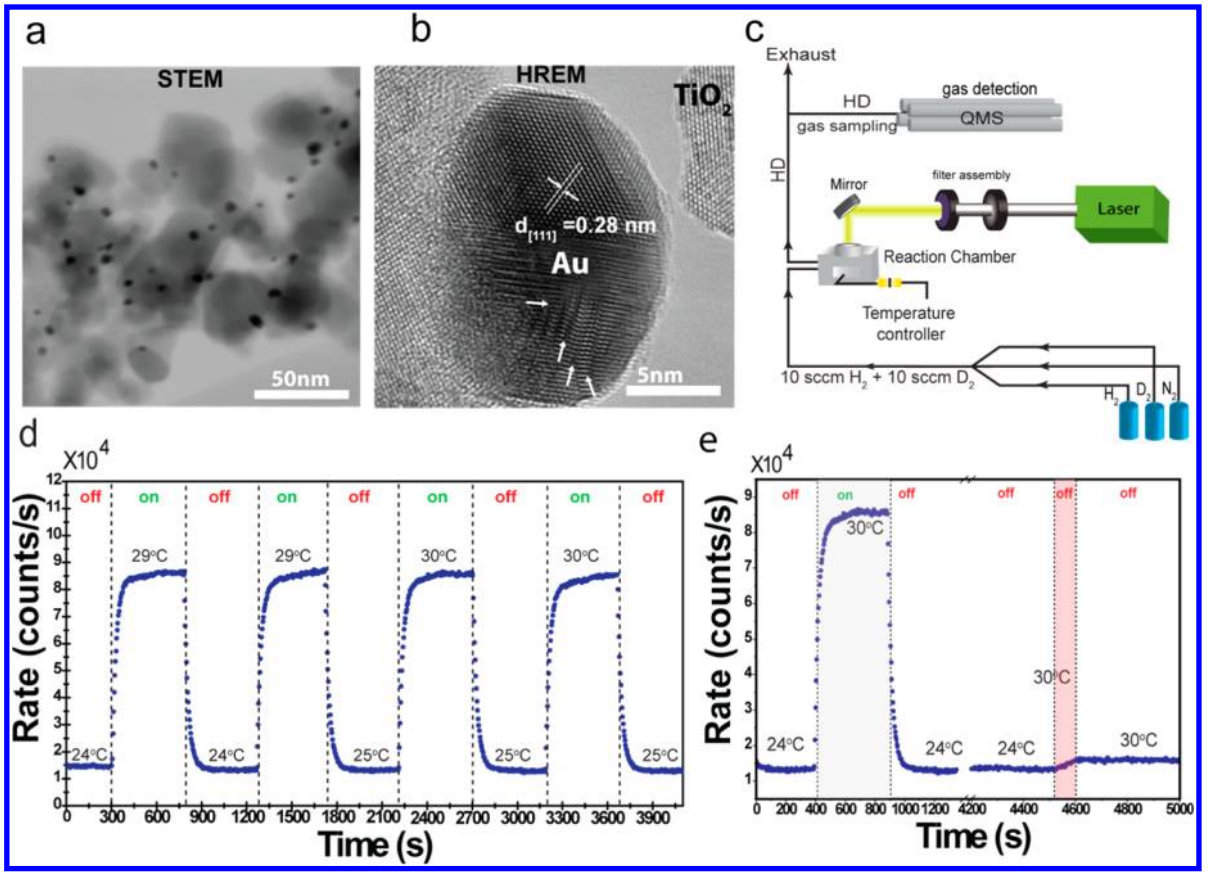

Figure 2. Plasmon-induced dissociation of H_2/D_2 using 1.75 wt % Au/TiO_2 photocatalyst at room temperature (297 K). (a) Scanning transmission electron micrograph showing distribution of 1.75 wt % AuNPs (dark particles) over a TiO_2 support (gray particles). (b) High-resolution transmission electron micrograph of a single Au NP supported on TiO_2 matrix showing darker contrast of Au NP as compared to TiO_2 support. Characteristic lattice fringes of Au (111) and (200) are visible at ~2.8 Å and 2.3 Å, respectively. (c) Schematic of overall experimental setup. (d) Real time monitoring of rate with laser excitation (on 2.41 W/cm^2) and without laser excitation (off). During 8 min of laser irradiation on the photocatalyst, the temperature increases by 5 K as shown in the figure, from 297 to 303 K. The dotted vertical lines indicate the laser on/off times. (e) Distinction between the photocatalytic rate (only laser on, 2.41 W/cm^2) and thermal heating rate (laser off, heating on). The shaded gray area displays the photocatalytic rate due to the laser. The shaded red area displays the rate of HD formation due to heating of the photocatalyst sample from room temperature (297 K) to 303 K without laser illumination.

of 20%.[12] Although this mechanism in principle offers the possibility of controlling the energy of the hot electron by varying the plasmon energy, the hot electrons are short-lived, undergo carrier multiplication through Auger-like processes, and eventually dissipate their energy to phonons, resulting in nanoparticle heating.[14,15]

Hot electron-induced femtochemistry on molecules absorbed on extended metallic surfaces has a long history.[15−18] Transient

dx.doi.org/10.1021/nl303940z | Nano Lett. 2013, 13, 240−247

hot electrons on metal surfaces can be formed from direct excitation using short pulse laser illumination. These hot electrons can transfer into specific electronic states of molecules adsorbed on the metal surface, inducing processes such as molecular dissociation, chemical reactions, and desorption.[19,20] The direct excitation of hot electrons on metal surfaces is a relatively inefficient process, requiring large incident light intensities to produce any appreciable effect.

In contrast, hot electron production from plasmon decay in nanoparticles is a much more efficient process.[10,21−25] The cross section for plasmon excitation is dramatically enhanced relative to the cross section for direct EHP excitation. For a nanoparticle whose size is much smaller than the wavelength of the plasmon resonance, all energy absorbed by the nanostructure will result in hot electron formation. Pioneering applications of hot electron-induced photochemistry on nanoparticles have recently been demonstrated in gas phase heterogeneous catalysis for the oxidation of ethylene on Ag nanocubes,[7] DNA melting,[26] nanowire catalysis,[27] and water splitting.[28,29]

In this study, we report the first experimental evidence of room temperature photocatalytic dissociation of H_2. The reaction can only be enabled by hot electrons generated by surface plasmon decay from small Au nanoparticles (Figure 1d−f). We chose the Au nanoparticle substrate because it does not dissociate H_2 under equilibrium conditions. The binding energy and sticking coefficient of H_2 on gold is very small and the molecules would not adsorb on a pure gold surface. To increase H_2 accommodation, the gold nanoparticles were supported on TiO_2. The TiO_2 matrix, into which H_2 diffuses, provides a passive function, ensuring that the H_2 molecules remain for a sufficiently long time near the Au surface to allow for hot electron transfer into an antibonding dissociative molecular resonance.[30] A fraction of the hot electrons created by resonant excitation of a plasmon transfer into the H_2 $1\sigma_u^*$ resonance, inducing H_2 dissociation. We indirectly measure the dissociation by exposing the nanoparticle substrate to a mixture of H_2 and D_2 and detecting the HD formation rate over a range of laser excitation intensities and wavelengths. This photocatalytic dissociation at room temperature is thus only accomplished by the hot electrons generated by the small AuNPs without applying any other source of energy, for example heat. The rate was also found to be strongly dependent on the concentration and on the size of the Au nanoparticles. The results are supported by state-of-the art first principles density functional theory (DFT) and embedded correlated wave function calculations.

Experiment. Au/TiO_2 photocatalyst samples were prepared using a wet chemical deposition precipitation method (Supporting Information, Section S1). In Figure 2a and b, high resolution transmission electron micrograph (HRTEM) images of a typical photocatalyst with 1.75 wt % Au loading are shown. Seven different samples were prepared with a range of Au nanoparticle sizes and concentrations (see also Supplementary Figures S1 and S2). The binding energies of the Au 4*f* peaks were measured using X-ray photoelectron spectroscopy to verify the elemental state of Au and to identify the percentage of Au present in the TiO_2 matrix (Supplementary Figure S3). UV−vis diffuse reflectance spectra of the samples show that the Au nanoparticle dipolar plasmon resonance is at 540−550 nm (Supplementary Figure S4.). The inhomogeneous broadening observed in these measurements can be attributed to the nanoparticle size distribution and the inhomogeneity of the surrounding TiO_2 matrix.

The photocatalyst samples were loaded into a stainless steel reaction chamber equipped with a 1 cm diameter quartz glass window through which the laser can illuminate the sample (Figure 2c). Ultrahigh-purity H_2 and D_2 gases were flowed into the reaction chamber, while light from a supercontinuum laser source was filtered and used to excite the Au nanoparticle plasmon over a range of intensities and frequency bands (Supplementary Figure S5). The overall reaction is:

$$H_2(g) + D_2(g) \rightarrow 2HD(g)$$

Results and Discussion. The rate of formation of HD with and without visible laser excitation (2.4 W/cm^2) with the photocatalyst sample (1.75 wt % Au loading) at room temperature (297 K) and atmospheric pressure is shown in Figure 2d. Initially, without illumination, a weak steady background rate of HD formation is observed at room temperature (297 K). This is due to a slow rate of dissociation of H_2 and D_2 at reactive sites, such as lattice imperfections, steps, and kinks, on the Au NP surface. The walls of the reaction vessel and flow tubes may also contribute to this background signal. After an initial steady HD baseline was observed, the substrate was excited using a supercontinuum laser source for 8 min. An almost instantaneous 6-fold increase in the rate of HD formation was observed. This photocatalytic rate enhancement for small Au NPs is significant, as under equilibrium conditions H_2/D_2 cannot dissociate on bulk Au at room temperature at all.[31] During the 8 min laser excitation period, the temperature of the substrate increased by 5K to 303K due to laser heating. After 8 min of illumination, the HD formation rate reached a steady state; then the laser was switched off, and the system reverted back to its initial rate and initial catalyst temperature, showing reversibility of the process.

To confirm that the photocatalysis process is not due to heating, the temperature of the sample was slowly increased from room temperature (297 K) to 303 K under dark conditions, corresponding to the observed temperature increase during laser illumination (pink area in Figure 2e). In this case, only a slight increase (1.2 fold) in HD generation rate was observed, far smaller than the increased rate observed under laser illumination. We can also rule out direct photodissociation of H_2, which would require much larger laser intensities (10^{13-14} W/cm^2).[32] A more detailed discussion of the elimination of heat- or local field-induced mechanisms is presented in the Supporting Information (Sections S6 and S7).

A systematic study was performed to determine the dependence of the photocatalytic rate on nanoparticle concentration and size (Figure 3). Five different Au/TiO_2 samples with small Au nanoparticles were prepared with increasing amounts of Au nanoparticle loading (0.57, 1.00, 1.75, 2.25, and 3.23 wt %). Three additional substrate samples with larger Au nanoparticles were prepared with 1, 0.9, and 1.8 wt % Au loading. The structure, morphology, and XPS spectra of all photocatalyst samples are provided in the Supporting Information (Figures S2 and S3).

In Figure 3a we observe a steady increase of photocatalytic rate with increasing Au loading, showing a strong dependence on Au nanoparticle concentration for HD generation. These experiments were performed using the same experimental conditions as shown in Figure 2c. The average HD formation rate was obtained by subtracting the background rate (laser off) from the photocatalytic rate (laser on) over four continuous runs on each sample. The strong dependence of the rate on nanoparticle concentration observed here has also been observed for other

dx.doi.org/10.1021/nl303940z | *Nano Lett.* 2013, 13, 240−247

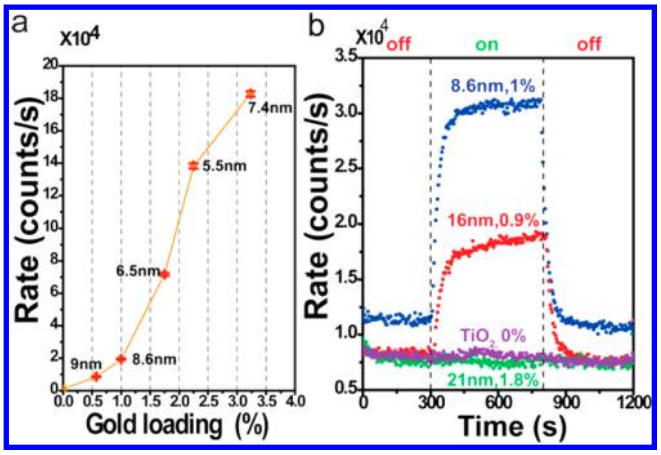

Figure 3. Dependence of photocatalytic HD generation on Au NP concentration and Au nanoparticle size. (a) Average photocatalytic (laser on) rate of HD formation at room temperature as a function of AuNP loading (shown as wt %). The mean AuNP sizes corresponding to the Au concentrations are shown beside each data point. The error bars are calculated as the standard deviation of the instrumental error in mass spectroscopic measurements. Overall size distributions of all the measured samples can be found in Supplementary Figure S1. (b) Dependence of the rate of HD formation on AuNP sizes. No photocatalytic rate was observed beyond a mean AuNP size of 20 nm or higher. No photocatalytic rate was observed for pristine TiO_2.

heterogeneous photochemical processes.[5] The extent of the rate increase also depends on Au NP size. The photocatalytic rate rises sharply with increasing Au loading from 1.75% to 2.25% with a reduction in mean nanoparticle diameter from 6.5 nm to 5.5 nm. However, with the same incremental increase in Au loading concentration from 0.5% to 1% for 9 nm diameter particles, the observed increase in HD generation rate was smaller. A similar size dependence was also observed for 2.25% to 3.23% Au loading, where the rate increase was much less pronounced for an increase in mean nanoparticle diameter from 5.5 to 7.4 nm.

Figure 3b shows the rate dependence on Au nanoparticle size for the same illumination laser intensity (2.41 W/cm^2). For the same Au nanoparticle loading (~1 wt %), the photocatalytic rate for 16 nm Au nanoparticles was only half that of 8.6 nm particles. Most significantly, the photoreactivity rate was negligible for Au nanoparticles larger than 21 nm, despite an almost 2-fold increase in Au nanoparticle concentration (1.8 wt %). The background self-dissociation rate was also significantly reduced in the presence of larger diameter Au nanoparticles.

This rapid decrease in dissociation rate with increasing Au nanoparticle size is certainly related to the decrease in available Au surface area:[5,33] for spherical nanoparticles, the ratio of surface to volume increases as the reciprocal of the nanoparticle radius. However, it is also likely that the sticking and chemisorption probability of H_2 to the Au nanoparticle plays a role. Smaller Au clusters (<3 nm) are known to be highly reactive due to the existence of a larger fraction of Au surface atoms with low coordination numbers.[34−36] In the present study, although the sizes of our Au nanoparticles are an order of magnitude larger than AuNP clusters, surface defects are still present (Figure 2b) which may be important for hydrogen adsorption and dissociation.[37−39] The dramatic dependence of photocatalytic rate on Au NP size and concentration shows that the process is indeed caused by the presence of the Au NP. Pristine TiO_2 (0% Au loading) under the same experimental conditions shows negligible HD production (Figures 3a and b).

The dependence of the room temperature photocatalytic rate on laser intensity is shown in Figure 4a. Four different substrates

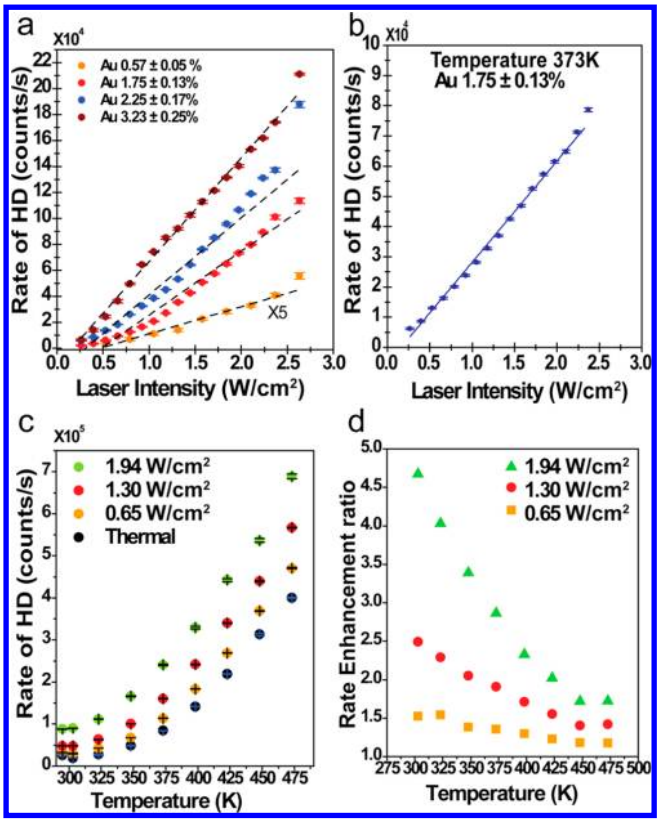

Figure 4. Dependence of photocatalytic rate on laser intensity and temperature. (a) The photocatalytic rate dependence (laser on) on the laser intensity at room temperature without any temperature control. Photocatalytic rates of four different samples with increasing wt % Au were studied for intensity dependence (see color code in the legend). Linear fits of the data points are shown as black dashed lines. Superlinear behavior at very high laser intensities is observed. (b) Dependence of the photothermal rate using 1.75 wt % Au/TiO_2 as a function of intensity of the laser at a fixed temperature of 373 K showing linear dependence of rate to laser intensity. (c) The effect of temperature on the photothermal process using 1.75 wt % Au/TiO_2. The thermal rate of HD formation was measured at different temperatures in the dark (heat, laser off) represented as black dots. The photothermal rate (heat, laser on) was measured with three different laser intensities at specific temperatures. Error bars are calculated as the standard deviation of the instrumental error in mass spectroscopic measurements. (d) Photothermal rate enhancement ratio as a function of operating temperatures using three different laser intensities.

(Au loading 0.57, 1.75, 2.25, and 3.23 wt %) were studied. The intensity dependence is essentially linear, with a slight superlinear increase at the highest illumination intensities due to laser heating (Figure 4a). Figure 4b shows the intensity dependence of the photocatalyst (1.75 wt %) at constant temperature of 373 K (Supplementary Figure S5). This higher constant temperature measurement eliminated the small thermal offset induced by laser heating and resulted in a linear dependence of the photocatalytic rate on laser intensity. Our observation of this linear rate dependence (Figure 4a and b) rules out both one- and two-photon excitation of electrons in the TiO_2 as the cause of the observed photodissociation.

dx.doi.org/10.1021/nl303940z | Nano Lett. 2013, 13, 240−247

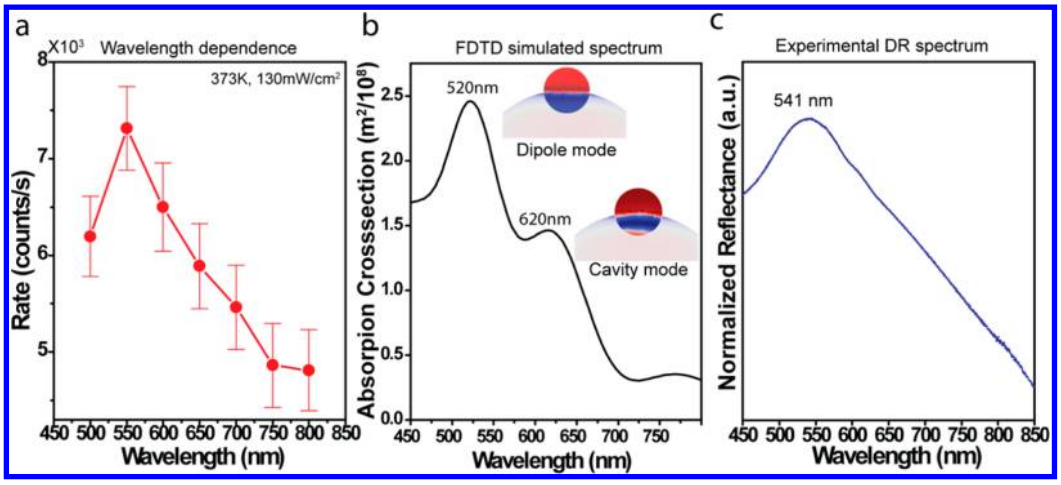

Figure 5. Wavelength dependence of photocatalytic rate. (a) Rate of HD formation at T = 373 K as function of a series of band-pass filter wavelengths, each adjusted to an intensity of 130 mW/cm^2. Au/TiO_2 photocatalyst with 1.75 wt % Au loading was used. Error bars were calculated as the standard deviation of the instrumental error in mass spectroscopic measurements. (b) Simulated absorption cross section spectrum of an Au/TiO_2 photocatalyst modeled as 7 nm AuNP attached to 30 nm TiO_2NP featuring a dipolar plasmon mode at 520 nm and a cavity plasmon mode at 620 nm. Inset shows corresponding charge plots (see Supporting Information, Section S7 for near-field plots). (c) Diffuse reflectance spectrum of powdered photocatalyst (1.75 wt % Au) sample showing the dipole resonance peak located at 541 nm. The location and shape of the plasmon peak are modified by inhomogeneous broadening.

In Figure 4c the combined effects of temperature and photon flux on the HD production rate are shown. The sample (1.75 wt %) was kept at different temperatures, and the steady-state rate of HD formation at each temperature was measured without and with laser excitation for three different laser intensities (0.65, 1.3, and 1.94 W/cm^2). Photothermal processes generated a significantly higher yield of HD than thermal heating alone. A rate enhancement ratio defined as the ratio of the photothermal to the thermal rate,[7] plotted as a function of temperature (Figure 4d), shows a 5- and 2-fold increase in enhancement at low and high temperature ranges, respectively. Therefore, one straightforward strategy to improve the HD yield would be to increase the substrate temperature: the hot electron yield also increases at higher temperatures.[40] However, the photoenhancement at ambient temperature is already quite substantial, indicating that plasmon-induced dissociation offers an alternative approach for enhancing photocatalyst activity.

The wavelength dependence of the photocatalytic rate was measured at a constant temperature of 373 K. Seven bandpass filters ranging from 500 to 800 nm, each with a wavelength spacing of 50 nm, were used. For each filter the transmitted light intensity was adjusted to 130 mW/cm^2 (Supporting Information, Section S5). The wavelength dependence of HD generation is shown in Figure 5a and compares very well with the calculated absorption cross section of 7 nm AuNP/30 nm TiO_2 (Figure 5b) and with the diffuse reflectance spectrum (Figure 5c). Since the absorption cross section corresponds directly to the hot electron production rate, this provides direct evidence for plasmon-induced hot electron-driven H_2 photodissociation. We also show that the effect of H_2 spillover is negligible for any shift or manipulation of the TiO_2 bandgap, implying that it remains virtually unaffected over the course of the experiment (Supporting Information, Section S10).

Proposed Mechanism. To investigate the feasibility of hot electron transfer from the Au NP to the antibonding $1\sigma_u$* state of an adsorbed H_2 molecule, DFT and embedded correlated wave function calculations were performed. The Au NP surface was modeled as a close-packed Au (111) facet.[41] This simple, idealized model of the Au NP is used to calculate the charge on H_2 as it approaches the Au surface and the associated ground and excited state potential energy surfaces. As H_2 approaches the Au surface from 5 to 2 Å away, both its bonding (B) and antibonding (AB) states shift down in energy (see arrows in Figure 6a, top panel). This energy gain is offset by a repulsive orthogonalization energy due to the overlap of the molecular states with the filled Au d-orbitals ($5d^{10}$).[31] This Pauli repulsion is particularly high for Au due to the large coupling matrix elements.[41] Even without the hot electrons, the downshift of the AB $1\sigma_u$* state causes it to become partially occupied (Figure 6b; see also Supplementary Figure S10). Interaction with the reducible (due to oxygen vacancies) TiO_2 substrate should make this effect even more pronounced, as a small, additional negative charge is transferred to the Au cluster from the oxide.[42] Indeed, separate investigations of an isolated H_2^- molecule reveal a metastable resonance associated with an occupied $1\sigma_u$* orbital nominally 1.7 eV above the ground state of neutral H_2[43] (Supplementary Figure S9). This Feshbach resonance broadens considerably as the molecule approaches the Au surface and hybridizes with the *s*-band electrons, ultimately leading to a finite occupation probability of $1\sigma_u$*, yielding a partially occupied antibonding state (Figure 6a and b).

Figure 6c shows the equilibrium ground state potential energy surface of H_2 on Au, clearly showing a steep rise in energy as H_2 approaches the surface (Figure 6c), strongly suppressing dissociative adsorption. For this reason, H_2 and D_2 will only weakly physisorb due to van der Waals forces with a physisorption well of 35−45 meV.[44,45] To dissociate H_2, the AB Feshbach resonance should overlap the hot electron distribution. Populating the Feshbach resonance will substantially weaken the H_2 bond and ultimately lead to dissociation. The excited state potential energy surface (Figure 6d and Supporting Information, Section S8) features an excitation energy of 1.8 eV above the ground state, which is the vertical energy difference of this excited state from the ground state minimum (Figure 6c, d). Hot electrons with energies greater than 1.8 eV should be able to transfer into a higher vibrational state of the molecule. In addition, in this excited state the H_2

dx.doi.org/10.1021/nl303940z | *Nano Lett.* 2013, 13, 240−247

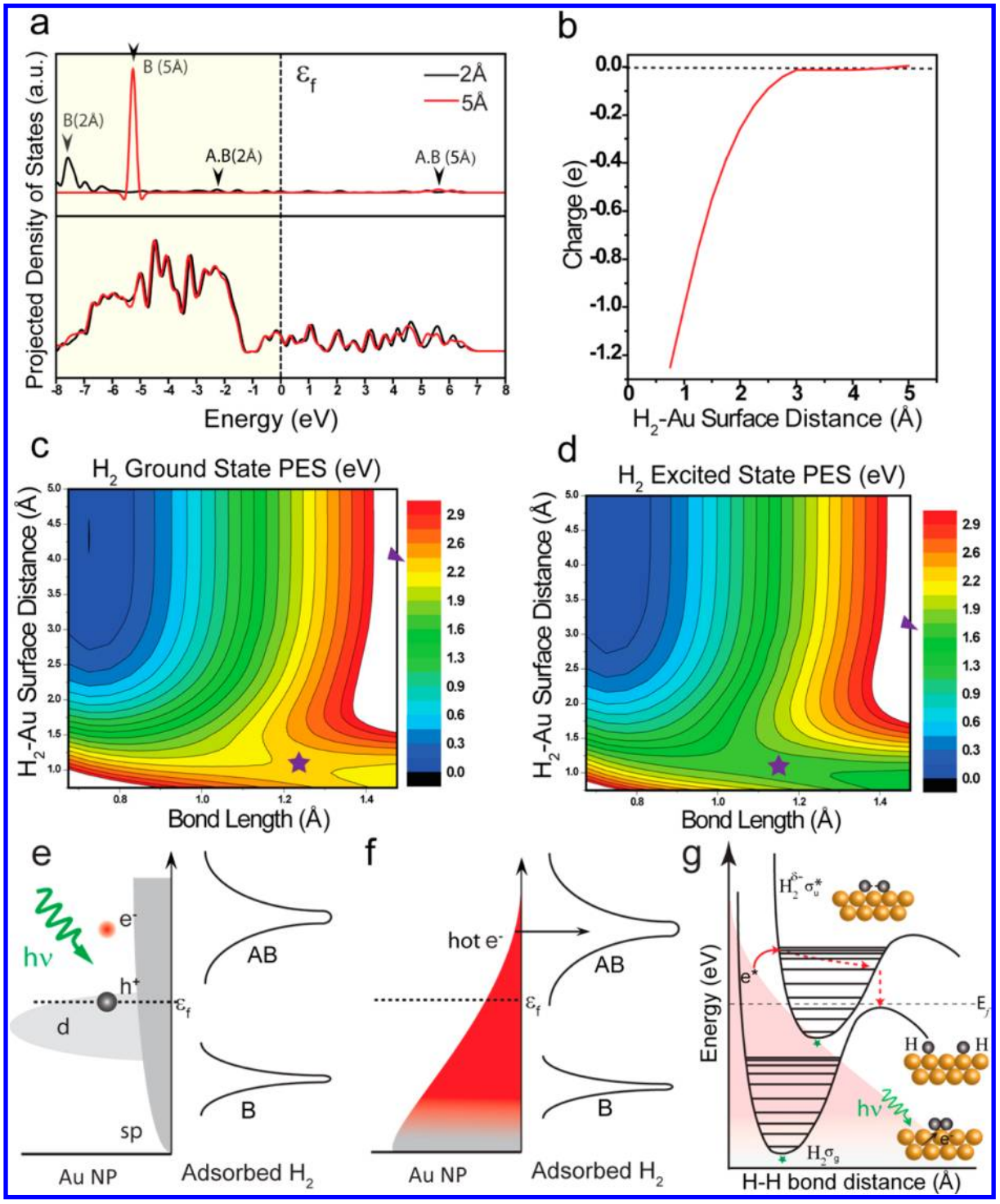

Figure 6. Mechanism of hot electron-induced dissociation of H_2 on Au. (a) Electronic density of states (DOS) of H_2 approaching a Au (111) surface using DFT, at different surface distances (see inset), projected onto one approaching atomic H atom (top panel) and total DOS (bottom panel). H_2 bond length is 0.725 Å. The dashed line marks the Fermi energy. Arrows denote the bonding (B) and antibonding state (AB) of H_2. (b) Ground state embedded CI-Singles (ECIS) Löwdin charge analysis as a function of H_2−Au surface distance. (c) ECIS ground state potential energy surface (PES) of H_2 on Au (111). Interaction with the surface can lead to dissociation at small distances only via high potential barrier of 2.3 eV (marked *). (d) ECIS sixth excited state PES of H_2 on Au showing lower dissociation barrier of 1.7 eV (marked *). Vertical excitation energy from the ground state minimum is only 1.8 eV. (e) Schematic of hot electron excitation in AuNP showing: d-band electron−hole pair excited above the Fermi level upon plasmon decay. The narrow bonding and broad antibonding states of adsorbed H_2 are denoted as B and AB, respectively. (f) Schematic of Fermi−Dirac type distribution of hot electrons permitting hot electron transfer into the antibonding state of H_2. (g) Proposed mechanism of hot-electron induced dissociation of H_2 on AuNP surface.

dissociation barrier was found to be substantially reduced to 1.7 eV, as compared to 2.3 eV in the ground state.

In a step-by-step representation of the mechanism (Figure 6e−g), hot electrons are initially optically excited at the AuNP

dx.doi.org/10.1021/nl303940z | *Nano Lett.* 2013, 13, 240−247

surface (Figure 6e). Each plasmon quantum will decay into a single EHP. The hot electrons soon lose coherence and form a nonequilibrium Fermi−Dirac type distribution which thermalizes by Auger scattering (Figure 6f). The hot electrons in the high energy tail of this distribution have sufficient energy to transfer into the antibonding state of the H_2 molecule, creating a transient negative ion (TNI), $H_2^{\delta-}$. This TNI will be stabilized by its image potential. On small Au nanoparticles, the lifetimes of the initially generated hot electrons can be much longer (100−500 fs) than on extended substrates because of increased confinement and reduced electron−electron interactions.[24,46] This provides sufficient time for the TNI to travel on the excited state potential energy surface, possibly in vibrationally excited states, extending its bond length (Figure 6g). Then the TNI transfers the electron back to the AuNP surface, where it returns to the ground-state potential energy continuum and dissociates.

Conclusions. This work demonstrates an important application of plasmonics to the field of heterogeneous photocatalysis, enabling the room temperature dissociation of H_2 on Au nanoparticles. We show that hot electrons, created from plasmon decay, can transfer into a closed shell H_2 molecule and induce dissociation. This effect provides a path for the optical control of chemical reactions. By tuning the plasmon resonances of metallic nanoparticles appropriately, it may be possible to populate specific electronic states of molecules adsorbed on the nanoparticle surface. This state-selective population of adsorbate resonances could be exploited to prepare reactants in specific states on nanoparticle surfaces, thus enabling an unprecedented, all-optical control of chemical reactions.

Methods. *Au/TiO_2 Photocatalyst Sample Preparation.* The Au/TiO_2 photocatalyst samples of different Au concentrations and AuNP sizes were prepared by the deposition−precipitation method using 1(M) NaOH as the basification agent, different amounts of $HAuCl_4 \cdot 3H_2O$ and maintaining the solution at different pH conditions. The photocatalyst solution was kept overnight at 100 °C in an oven for drying, and the next day the dried samples were sintered inside the oven at 300 °C for 2.30 h. Subsequently the photocatalyst samples were cooled avoiding the presence of oxygen and moisture and immediately loaded into the reaction chamber for the experiment (see Supporting Information for details and references). The size and morphology of the catalyst samples were imaged using JEOL 2100 field emission gun transmission electron microscope (JEM 2100F TEM). PHI Quantera XPS was used to identify the Au content and electronic state, and a Cary UV−Vis 5000 equipped with Harrick Scientific diffuse reflectance accessory was used to measure the optical spectra of photocatalysts.

Measurement Techniques. The photocatalysis reaction was performed in a temperature-controlled, sealed stainless steel reaction vessel equipped with a quartz window. The rate measurements were done using a Hiden HPR 20 high resolution quadrupole mass spectrometer. The photocatalyst sample was loaded inside the chamber and 10 sccm of H_2 and 10 sccm of D_2 were flown inside the chamber, while laser light was shined into the chamber through the quartz window. The laser was turned on into the chamber for 7−10 min (laser on) followed by 7−10 min in the dark (laser off). The net photocatalysis rate was measured as a difference between the standard deviations of laser on data points and laser off data points to get rid of any baseline.

To perform intensity-dependent experiments, the laser intensity was controlled using a set of neutral density filters.

Wavelength dependence experiments were performed (within the range of 450−1000 nm) using different band-pass filters ranging from 500 to 800 nm in steps of 50 nm. A temperature controller was used to keep the photocatalyst at different temperatures ranging from 24 to 200 °C. (See Supporting Information S5 for details of the procedure.)

First Principles Calculations. We perform a PAW DFT calculation using VASP on a Au(111) slab. To obtain a correlated wave function correction, as well as electronically excited states, we cut out a finite sized gold cluster of 14 Au atoms from the surface. We then embed the cluster using a DFT-derived local embedding potential, calculated following an embedding approach by Huang et al.[47,48] The difference between a high-level correlated wave function method and an embedded DFT calculation on the cluster gives rise to a correction to the pure DFT results. As high-level methods, we consider both CI-Singles calculations of 10 excited states from an RHF ground state, as well as a state-averaged CASSCF calculation. (For details, see Supporting Information, Section S8.)

Electromagnetic Simulations. We used the finite-difference time-domain method (Lumerical FDTD Solutions) to calculate the far-field and the near-field properties of the Au/TiO_2 nanoparticles. The charge density distributions have been calculated and generated using the finite element method (Comsol Multiphysics). The bulk dielectric function tabulated by Johnson and Christy has been used for gold,[49] and a dielectric constant of 2.75 has been used for Rutile (R-TiO_2).[50] Calculations have been performed in air and for a longitudinal polarized excitation. Geometrical parameters have been extracted from microscopy images and size distribution statistics. In our model, the Au NP is taken spherical and is considered semiembedded in a spherical R-TiO_2 NP. FDTD calculations have been performed for several typical size parameters extracted from experimental data (cf. Supplementary Figures S6 and S7). Systematic calculations have been done varying the Au-NP size, the TiO_2−NP size, and the dielectric constant of TiO_2.

■ ASSOCIATED CONTENT

Ⓢ Supporting Information

Au/TiO_2 photocatalyst sample preparation, characterization of structure and morphology, spectroscopic characterization, experimental setup, experimental procedure, effect of plasmonic heating, local field enhancement, first principles calculations, isotope effect, stability of photocatalyst, and effect of spillover. This material is available free of charge via the Internet at http://pubs.acs.org.

■ AUTHOR INFORMATION

Corresponding Author

*E-mail: halas@rice.edu; nordland@rice.edu.

Notes

The authors declare no competing financial interest.

■ ACKNOWLEDGMENTS

This research was supported by the Robert A. Welch Foundation under grants C-1220 (N.J.H.) and C-1222 (P.N.) ,the Air Force Office of Scientific Research (AFOSR) FA9550-10-1-0469, the Office of Naval Research (EAC) and National Science Foundation (EAC), as well as the Max Kade Foundation, New York. We acknowledge Yang Cao, Dr. Heidar Sobhani, Yu Zhang, Dr. Na Liu, Jared Day, Mark Knight, Bob Zheng and Dr. Alex Urban, and Nick King for proof reading the manuscript and useful discussions. We also acknowledge Bruce Brinson, Wen Guo, and Bo Chen for help with TEM imaging and XPS

measurements, Prof. G. Kresse for help with VASP, and Mark Buckley and Ian Tyrer-Tomkinson from Hiden Analytical for their guidance with quadrupole mass spectroscopic measurements. S.M. carried out the wet-chemical synthesis of photocatalysts, mass spectrometer measurements, and data analysis. O.N. and L.B. did structural and elemental analysis of the experimental samples, F.L. and J.C. did DFT and ECIS calculations, and N.L. did FDTD simulations. B.L. helped in building the optical setup.

REFERENCES

(1) Linic, S.; Christopher, P.; Ingram, D. B. *Nat. Mater.* **2011**, *10* (12), 911−921.
(2) Lee, J.; Mubeen, S.; Ji, X.; Stucky, G. D.; Moskovits, M. *Nano Lett.* **2012**, *12* (9), 5014−5019.
(3) Silva, C. G.; Juarez, R.; Marino, T.; Molinari, R.; Garcia, H. *J. Am. Chem. Soc.* **2011**, *133* (3), 595−602.
(4) Ingram, D. B.; Linic, S. *J. Am. Chem. Soc.* **2011**, *133* (14), 5202−5205.
(5) Murdoch, M.; Waterhouse, G. I. N.; Nadeem, M. A.; Metson, J. B.; Keane, M. A.; Howe, R. F.; Llorca, J.; Idriss, H. *Nat. Chem.* **2011**, *3* (6), 489−492.
(6) Seh, Z. W.; Liu, S.; Low, M.; Zhang, S.-Y.; Liu, Z.; Mlayah, A.; Han, M.-Y. *Adv. Mater.* **2012**, *24* (17), 2310−2314.
(7) Christopher, P.; Xin, H.; Linic, S. *Nat. Chem.* **2011**, *3* (6), 467−472.
(8) Hung, W. H.; Aykol, M.; Valley, D.; Hou, W.; Cronin, S. B. *Nano Lett.* **2010**, *10* (4), 1314−1318.
(9) Hou, W.; Hung, W. H.; Pavaskar, P.; Goeppert, A.; Aykol, M.; Cronin, S. B. *ACS Catal.* **2011**, *1* (8), 929−936.
(10) Knight, M. W.; Sobhani, H.; Nordlander, P.; Halas, N. J. *Science* **2011**, *332* (6030), 702−704.
(11) Goykhman, I.; Desiatov, B.; Khurgin, J.; Shappir, J.; Levy, U. *Nano Lett.* **2011**, *11* (6), 2219−2224.
(12) Fang, Z.; Liu, Z.; Wang, Y.; Ajayan, P. M.; Nordlander, P.; Halas, N. J. *Nano Lett.* **2012**, *12* (7), 3808−3813.
(13) Fang, Z.; Wang, Y.; Liu, Z.; Schlather, A.; Ajayan, P. M.; Koppens, F. H. L.; Nordlander, P.; Halas, N. J. *ACS Nano* **2012**, *6*, 10222−10228.
(14) Chen, J. K.; Tzou, D. Y.; Beraun, J. E. *Int. J. Heat Mass Transfer* **2006**, *49* (1−2), 307−316.
(15) Frischkorn, C.; Wolf, M. *Chem. Rev.* **2006**, *106* (10), 4207−4233.
(16) Ho, W. *J. Phys. Chem.* **1996**, *100* (31), 13050−13060.
(17) Gadzuk, J. W. *Phys. Rev. Lett.* **1996**, *76* (22), 4234−4237.
(18) Gadzuk, J. W. *Chem. Phys.* **2000**, *251* (1−3), 87−97.
(19) Bonn, M.; Funk, S.; Hess, C.; Denzler, D. N.; Stampfl, C.; Scheffler, M.; Wolf, M.; Ertl, G. *Science* **1999**, *285* (5430), 1042−5.
(20) Avouris, P.; Walkup, R. E. *Annu. Rev. Phys. Chem.* **1989**, *40* (1), 173−206.
(21) Hofmann, J.; Steinmann, W. *Phys. Status Solidi B* **1968**, *30* (1), K53−K56.
(22) Inagaki, T.; Kagami, K.; Arakawa, E. T. *Phys. Rev. B: Condens. Matter* **1981**, *24* (6), 3644−3646.
(23) Endriz, J. G.; Spicer, W. E. *Phys. Rev. Lett.* **1970**, *24* (2), 64−68.
(24) Watanabe, K.; Menzel, D.; Nilius, N.; Freund, H.-J. *ChemInform* **2006**, *37*, (52), 10.1002/chin.200652229.
(25) Lehmann, J.; Merschdorf, M.; Pfeiffer, W.; Thon, A.; Voll, S.; Gerber, G. *Phys. Rev. Lett.* **2000**, *85* (14), 2921−2924.
(26) Huschka, R.; Zuloaga, J.; Knight, M. W.; Brown, L. V.; Nordlander, P.; Halas, N. J. *J. Am. Chem. Soc.* **2011**, *133* (31), 12247−12255.
(27) Sun, M.; Xu, H. *Small* **2012**, *8* (18), 2777−2786.
(28) Thomann, I.; Pinaud, B. A.; Chen, Z.; Clemens, B. M.; Jaramillo, T. F.; Brongersma, M. L. *Nano Lett.* **2011**, *11* (8), 3440−3446.
(29) Chen, H. M.; Chen, C. K.; Chen, C.-J.; Cheng, L.-C.; Wu, P. C.; Cheng, B. H.; Ho, Y. Z.; Tseng, M. L.; Hsu, Y.-Y.; Chan, T.-S.; Lee, J.-F.; Liu, R.-S.; Tsai, D. P. *ACS Nano* **2012**, *6* (8), 7362−7372.
(30) Wei, J.; Ji, H.; Guo, W.; Nevidomskyy, A. H.; Natelson, D. *Nat. Nano* **2012**, *7* (6), 357−362.
(31) Hammer, B.; Norskov, J. K. *Nature* **1995**, *376* (6537), 238−240.
(32) Ludwig, J.; Rottke, H.; Sandner, W. *Phys. Rev. A: At. Mol. Opt. Phys.* **1997**, *56* (3), 2168−2181.
(33) Fujitani, T.; Nakamura, I.; Akita, T.; Okumura, M.; Haruta, M. *Angew. Chem., Int. Ed.* **2009**, *48* (50), 9515−9518.
(34) Lopez, N.; Janssens, T. V. W.; Clausen, B. S.; Xu, Y.; Mavrikakis, M.; Bligaard, T.; Nørskov, J. K. *J. Catal.* **2004**, *223* (1), 232−235.
(35) Roduner, E. *ChemInform* **2006**, *37*, (39), 10.1002/chin.200639226.
(36) Hvolbæk, B.; Janssens, T. V. W.; Clausen, B. S.; Falsig, H.; Christensen, C. H.; Nørskov, J. K. *Nano Today* **2007**, *2* (4), 14−18.
(37) Fujita, T.; Guan, P.; McKenna, K.; Lang, X.; Hirata, A.; Zhang, L.; Tokunaga, T.; Arai, S.; Yamamoto, Y.; Tanaka, N.; Ishikawa, Y.; Asao, N.; Yamamoto, Y.; Erlebacher, J.; Chen, M. *Nat. Mater.* **2012**, *11* (9), 775−780.
(38) Scholl, J. A.; Koh, A. L.; Dionne, J. A. *Nature* **2012**, *483* (7390), 421−427.
(39) Li, Z. Y.; Young, N. P.; Di Vece, M.; Palomba, S.; Palmer, R. E.; Bleloch, A. L.; Curley, B. C.; Johnston, R. L.; Jiang, J.; Yuan, J. *Nature* **2008**, *451* (7174), 46−48.
(40) Lee, Y. K.; Jung, C. H.; Park, J.; Seo, H.; Somorjai, G. A.; Park, J. Y. *Nano Lett.* **2011**, *11* (10), 4251−4255.
(41) Santen, R. A. v.; Neurock, M. *Molecular Heterogeneous Catalysis: A Conceptual and Computational Approach*; Wiley-VCH: New York, 2006.
(42) Laursen, S.; Linic, S. *Phys. Rev. Lett.* **2006**, *97* (2), 026101.
(43) McWeeny, R. *J. Mol. Struct.: THEOCHEM* **1992**, *261* (0), 403−413.
(44) Nordlander, P.; Holmberg, C.; Harris, J. *Surf. Sci.* **1985**, *152−153* (Part 2), 702−709.
(45) Harten, U.; Toennies, J. P.; Woll, C. *J. Chem. Phys.* **1986**, *85* (4), 2249−2258.
(46) Link, S.; Burda, C.; Wang, Z. L.; El-Sayed, M. A. *J. Chem. Phys.* **1999**, *111* (3), 1255−1264.
(47) Libisch, F.; Huang, C.; Liao, P.; Pavone, M.; Carter, E. A. *Phys. Rev. Lett.* **2012**, *109*, 198303.
(48) Huang, C.; Pavone, M.; Carter, E. A. *J. Chem. Phys.* **2011**, *134* (15), 154110−11.
(49) Johnson, P. B.; Christy, R. W. *Phys. Rev. B: Condens. Matter* **1972**, *6* (12), 4370−4379.
(50) Fisher, J.; Egerton, T. A. Titanium Compounds, Inorganic. In *Kirk-Othmer Encyclopedia of Chemical Technology*; John Wiley & Sons, Inc.: New York, 2000.